Analysis of Furanic and Aromatic Structural Motifs in Hydrothermal Carbon

A Major Qualifying Project

Submitted to the faculty

Of the

Worcester Polytechnic Institute

For partial fulfillment of the requirements for the

Degree of Bachelor of Science

By

_____

Brendan McKeogh

May 1, 2015

Approved:

_____

Professor Michael T. Timko, Advisor

Abstract

Preliminary investigations into a promising new material, ball milled hydrothermal carbon, have shown long-lived radical defect groups on the surface as a result of the reaction. Raman spectroscopy indicated a process of aromatization and deoxygenation through condensing of alkyl branches and deoxygenation reactions. Confirmation of structural modifications of hydrochar would allow for the material to be better characterized for applications in catalysis and water remediation. To confirm structural modifications, hydrochars were prepared from glucose (a hexose sugar) and xylose (a pentose sugar) for comparison with structurally different hydrochars. Both char types were subjected to ball milling, a mechanochemical process, and analyzed with the use of both ATR-FTIR and DRIFT spectroscopies along with Raman Spectroscopy to understand the shift. IR spectroscopies indicated the expected shift towards a more aromatic material with decreasing oxygen functionalities, at the expense of alkyl and olefin groups. Sugar type played a large role in materials formed, with xylose forming a hydrochar with less olefin groups and increased amounts of sugar rings within the structure. Ball milling products shifted towards more aromatic in xylose and more olefin groups in glucose char. Future work to characterize ball milling is needed as IR is a qualitative technique and Raman fitting is based off graphitic models.

Table of Contents

Introduction

It is a well-established fact that human impact on global warming is both significant and increasing, caused by increased concentration of carbon dioxide, methane, and nitrous oxide in the atmosphere.[4] Carbon dioxide emission in particular is of concern, with the current trend in Co2 output and accumulation could mean sustained climate effects for the next 1000 years.[5] For these reasons there is an urgent need to address the accumulation of CO2. Since fossil fuel consumption accounts for about 80% of the anthropogenic Co2 released, a critical stance is necessary.[6] Fossil fuels encompasses coal, natural gas, and petroleum resulting from the decomposition of biomass. They are non-renewable resources and the carbon produced from these sources and the processes that create these substances are far slower than current usage. To address the harmful environmental impacts of fossil fuels, alternative energy source have emerged, such as solar panels, wind harvesting, and fuel cell technology. Biofuels are another such renewable energy source, and are especially appealing as the biofuel can be used as if it were petroleum based, enabling a smoother transition to alternative energy than fuel cell technology or electric vehicles.

Biofuels are liquids or gasses produced from biomass used for transportation energy [11]. According to the 2013 Renewable Energy Data Book produced by the U.S. Department of Energy, biomass based energy accounted for 5.5% of the total U.S energy produced, or 4.5 quadrillion Btu. Bio-ethanol is the largest biofuel currently produced it the U.S., produced primarily from corn via a fermentation reaction. This breaks down the high starch content of the corn. This approach is hindered by feedstock, which is only a small fraction of the total biomass available and it directly compete with food sources. Thermochemical processing sidesteps both these problems as it focuses on the degradation of lignocellulosic biomass, which comprises the vast majority of available biomass and does not directly compete with food sources.

Lignocellulosic biomass is comprised of 3 major polymeric constituents: cellulose, hemicellulose, and lignin. The cellulose is both the most uniform of the three materials and contains the highest energy density. Unfortunately, the molecular structure and nano and even micro structures of the lignocellulosic material make easy degradation of the cellulose a daunting task. Cellulose is a polymer of sugars in tightly packed crystalline micro fibrils within a hemicellulose matrix. Hemicellulose is a polymer of sugars, but has different sugar types and is not a tightly order as cellulose. Finally the cellulose and hemicellulose are surrounded by lignin, a strongly cross-linked aromatic polymer. The pretreatment stage in a thermochemical processing route needs to addresses this need such that reaction time can be efficient and targeted to smaller atoms. One cost-effective pretreatment method uses dilute sulfuric acid,

removing the hemicellulose. This has resulted in higher sugar yields, indicating possible cleaving of cellulose chains.[15] However this method would result in a sulfuric acid recycle and emission, which is to be avoided. A solid acid catalyst with acid groups on the surface could instead allow for recovery of the catalyst using a physical separation rather than a chemical separation, which would increase the economic viability of the entire process and also positively impact the environment. Hydrochar is a cheap and environmentally friendly carbon material that could realize the goal of a stable solid acid catalyst. Hydrochars are an amorphous oxygenated carbon species. It has a good degree highly tunable in morphology, size, surface area, and density of acid sites. [19 This is useful for optimization of the materials along with its ability to functionalize them. In the preceding MQP project, hydrothermal carbons were analyzed and subjected to ball milling to understand the process. Ball milling contacts char with grinding balls inside a milling vessel, localizing high pressure and high temperatures to contact the carbon. Ball milling enhances the reactivity of the carbon surface, creating long lived radical defect sites on the surface. [20]

Currently, this study aims to better characterize the structural and functional changes that occur with ball milling based off the work of Heckley, Toto, and Venegas. This study considers hydrothermal chars from glucose and xylose feedstock, and characterizes the materials via RAMAN analysis to track structural changes and IR spectroscopy to correlate structural changes and to observe functional changes. This work offers better characterization of hydrothermal char through RAMAN deconvolution and shows that IR can track changes in the material. This will contribute towards a good working structural model so that predictions to be made about the reactivity of the material during functionalization or adjustment of the synthesis of the material for optimized structure.

Experimental

Hydrothermal Carbonization of sugars and the subsequent preparation of hydrochars are explained. Following this the ball milling process for hydrochars is stated along with the studies conducted and the data displayed. Finally, ATR-FTIR, DRIFTS, and Raman spectroscopy theory, settings, and fittings and peak locations are located in their respective sections. Finally, uncertainty encountered as a result of the experiments is addressed in an uncertainty analysis section.

Hydrochar Synthesis via Hydrothermal Carbonization

Hydrothermal chars were prepared by the method described by Heckley et. al., in which 39.6 g of glucose or the molar equivalent in xylose (33.0 g) was dissolved into 160ml of deionized water, from which 100ml

was extracted.[20] The glucose was supplied by Fischer scientific BDI D+ glucose 99% and the xylose supplied by Acros Organics respectively. Solution was placed in a 160 mL Teflon-lined stainless steel autoclave. Glucose chars, unless otherwise specified, were placed in the oven for 5 hours while xylose chars were also reacted at 180 °C with a 24 hour oven duration. The oven was at ambient temperatures and the reaction times included heating the 180°C. At the end of the duration the oven was turned off and the vessel remained sealed in the oven until the vessel reached room temperature. The char was then washed and filtered using water and ethanol three times with 40 ml aliquots of each solvent. The char was then dried in a petri dish overnight in an oven at 80 °C. To prepare the char for testing it was ground into a powder with a mortar and pestle.

Ball Milling

Following the method described by Heckley et. al, 0.5 grams of the dried hydrochar was placed in a 10 mL stainless steel ball-milling vessel along with two 5 mm diameter stainless steel balls and one 10 mm diameter ball separating the other two. The vessel was sealed in an atmospheric environment by closing the lid to the body of the vessel silicone rubber O-ring on the gap. The vessel was compressed and the rubber O-ring was wrapped over with insulating tape. The vessel was loaded into a Retsch MM200 mixer mill and milled at an amplitude of 60 for the reaction time specified. At the conclusion of ball milling the vessel was removed from the mixer mill and cooled for around 20 minutes at room temperature before opening. Since milling balls and vessel were reused these were cleaned soon after the milling products were collected from the vessel to prevent corrosion of the equipment.

In the ball milling study hydrochar was divided and subjected to ball milling for a range of times. For glucose ball milling was done for time periods of 30, 60, 90, and 120 minute and analyzed with ATR-FTIR while another glucose study ball milled for 30, 60, and 120 minutes and analyzed under DRIFTS. Xylose chars were ball milled for 1 hour only to determine how reproducible the ball milled xylose chars are, due to small batch yields preventing time series. Xylose char was examined with ATR-FTIR and DRIFTS and with Raman Spectroscopy. DRIFTS were repeated once for each of the 3 samples taken from the char. A Raman spectrum was taken at 3 different locations then averaged together for a Raman curve.

Infrared Spectroscopy

Infrared spectroscopy measures the intensity of infrared rays that a substance absorbs for a given wavelength. Adsorption of the infrared occurs when the wavelength of the infrared beam matches the resonant frequency of a type of vibration in the solid. To better obtain high resolution spectra in both the high field area of 4000-2000 cm-1 and the fingerprint region of 1500-500 two different methods of FTIR

were used: Attenuated Total Reflectance Fourier Transform Infrared (ATR-FTIR) spectroscopy and Diffuse Reflectance Infrared Fourier Transform spectroscopy (DRIFTS). For both ATR-FTIR spectroscopy and DRIFTS the background and the samples were analyzed for the range of 4000-400 cm-1, a resolution of 2 cm-1, and an accumulation of 96 scans. A Berkin Elmer FTIR spectrometer was used for the ATR-FTIR, while DRIFTS was conducted on a Nicolet 560 Magna IR with a SpectraTech DRIFTS cell. For both techniques the background and the samples were analyzed for the range of 4000-400 cm-1, a resolution of 2 cm-1, and an accumulation of 96 scans.

Raman Spectroscopy

Raman spectroscopy measures the wavelength of light scattered from contact with a surface. If the wavelength of the returning light is the same as the incident light then the interaction is Rayleigh scattering. This is seen with motion such as translational molecular motion. The perpendicular scattering of light with an altered frequency is the signal picked up in Raman. The intensity and frequency provides knowledge about the compound, such as different groups or atoms. Raman spectroscopy works well to identify more symmetric or non-polar bonds, such as C-C or S-C. In this respect, it is quite useful for structural characterization of carbon materials.

Raman spectra of carbon materials shows 2 major bands that are widely used to gain structural information. Raman showed only one band for single crystal graphite band located at 1575 cm-1 and is named the G band. An additional band is seen at 1360 cm-1 in polycrystalline graphite, and is aptly named defective or the D band. [Cuesta, 28] Carbonaceous Raman spectra were proposed by Ferrari and Robertson to show structural changes in disordered carbon allotropes when compared against each other.
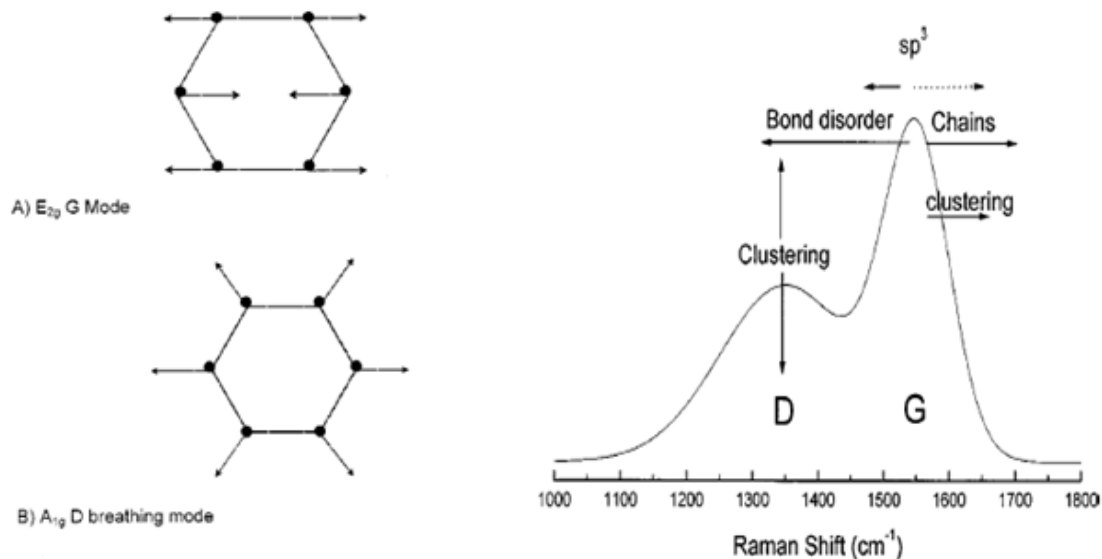
Figure 1: Raman Spectrum of D and G Peak areas (right) and trends for structure change/Raman relation.
Left shows the vibration modes for sp2 carbon (left) for Shuffling (G-mode, top) and Breathing (D-mode, bottom). Adapted from Ferrari and Robertson.[27]

While hydrochar is radically different to any disordered carbon created from graphite, the simple model of the intensity ratio Id/Ig of the D and G peaks was proposed as a measure of clustering. This is because the D breathing mode is only identified for 6 member aromatic ring structural components, such as small aromatic clusters. The E2g stretching mode was determined to not come exclusively from highly ordered graphite but also olefin groups.[Ferrari and Robertson] The G band was also noted to shift up field with the growth of olefin chains, which will also be used to assess the chars. For this model the D and G peak locations are not fixed and can be moved for optimal fitting. The second fitting model was the Sadezky et al, in which peak assignments were based off disordered graphite and soot. The D1 and D2 peaks were first determined from disordered graphite and the D3 and D4 were determined from the fitting of soot, which is amorphous carbon. This model is appealing as it is based off characterization of a type of burned carbon as opposed to graphite material which is inherently highly ordered and has virtually no oxygen content. Although the fitting of curves was done with Lorentzian peak fitting, these were not used in favor of Gaussian. For this method peak locations (in cm-1) are not fixed. Finally, the Li fitting for the compositions of pyrolyzed coals is used to deconvolute the spectra with 10 band assignments, shown in Table 3. The Li fitting was used to determine trends in structural change with ball milling.

Chars were prepared for Raman analysis by depositing fine particles as opposed to clots onto the glass slide. A Horiba XploRa Raman spectrometer was used with the settings described by Heckley et al. The laser wavelength was selected for 532 nm at 10% laser power. A 5 second accumulation time was run for 50 accumulations for a trial. The scan range was collected for 800-2200 cm-1. Gratings, slits, and holes of

1800, 300, and 100 respectively were selected. Fitting of the Raman plots was conducted using Magic Plot software. Fitting added tunable curves to the plot, which adds together with other fitting curves to make an overall fit for the data. The location of the curves were set, but the intensity and the width of the curves could be adjusted. The shape of the curves was selected as Gaussian fitting.

Table 1: Li et. al. Raman Fitting Assignments.

Band Name	Band Position (cm-1)	Description	Bond Type
GL	1700	Carbonyl group C=O	sp2
G	1590	Graphite E_{2g}^2, alkene C=C	sp2
GR	1540	aromatics with 3–5 rings, amorphous	sp2
VL	1465	methylene or methyl, semicircle breathing of aromatic rings, amorphous	sp2, sp3
VR	1380	methyl group, semicircle breathing of aromatic rings, amorphous	sp2, sp3
D	1300	D band on highly ordered carbonaceous materials, C–C between aromatic rings and aromatics with no less than six	sp2
SL	1230	aryl–alkyl ether, para-aromatics	sp2, sp3
S	1185	$C_{aromatic}$-C_{alkyl}, aromatic (aliphatic) ethers, C–C on hydroaromatic rings, hexagonal diamond carbon sp^3, C–H on aromatic rings	sp2, sp3
SR	1060	C–H on aromatic rings, benzene (ortho-disubstituted) ring	sp2
R	960-800	C–C on alkanes and cyclic alkanes, C–H on aromatic rings	sp2, sp3

Table 2: Sadezky et. al. Raman Fitting Assignments

Band Name	Band Position (cm-1)	Description	Bond Type
G	1580	Graphitic lattice (E2g-symmetry)	sp2
D1 (D)	1350	Disordered graphitic lattice (graphene layer edges, A1g symmetry)	sp2
D2 (D')	1620	Disordered graphitic lattice (surface graphene layers, E2g-symmetry)	sp2
D3 (D'')	1465	Amorphous carbon	sp2, sp3
D4 (I)	1380	Disordered graphitic lattice (A1g symmetry), polyenes, ionic impurities	sp2, sp3

Results & Discussion

The results are divided into 2 major sections. The first compares hydrochar to ball milling for glucose. The second section compares the xylose hydrochars to their ball milling products. The glucose char Raman fitting assignments are conducted with the data of Heckley et al, which were synthesized with the same process as the glucose chars produced through this study.

Glucose Hydrochar Ball Milling Time

Glucose hydrochar displays clear changes to the structure of the material with IR spectroscopy from this study and different fitting methods for Raman data. The data is then divided by analytical method used, which were DRIFTS then ATR-FTIR, followed by Raman fittings of the hydrochar and milling products.

Infrared Spectroscopy Analysis

The DRIFTS spectra shown in figure # above was used to characterize the 4000-2000 cm-1 range in which O-H and C-H bonds absorb. The broad band at 3450 cm-1 corresponds to the O-H stretching of water in the solid hydrochar. This happens in spite of drying of all hydrochars overnight and analyzing ball milled products shortly after synthesis. Ball milling products were all DRIFTS spectra collected showed a broad O-H stretch, though it does appear to decrease in size with ball milling. The band from about 3000-2800 cm-1 encompasses the major adsorption ranges of alkane C-H stretching. While the adsorption band does not show multiple bands, there is a sharp tip at 2925 cm-1, which is within the reported range for acyclic C-H stretching on carbon bonded to only 1 hydrogen.[Socrates] This peak

appears to decrease in area with ball milling, but not much. Finally, there is a weak band at around 2360 cm-1 for all spectra except the 60 minute ball milling, which has a strong inverted band. This is a spurious band corresponding to carbon dioxide. The bands and must have resulted from carbon dioxide entering the cell when samples were loaded, and the inverted band from not allowing the cell to have purged long enough for taking the background.

Figure 2: DRIFTS of Glucose Hydrochar and ball milling products of different time intervals.
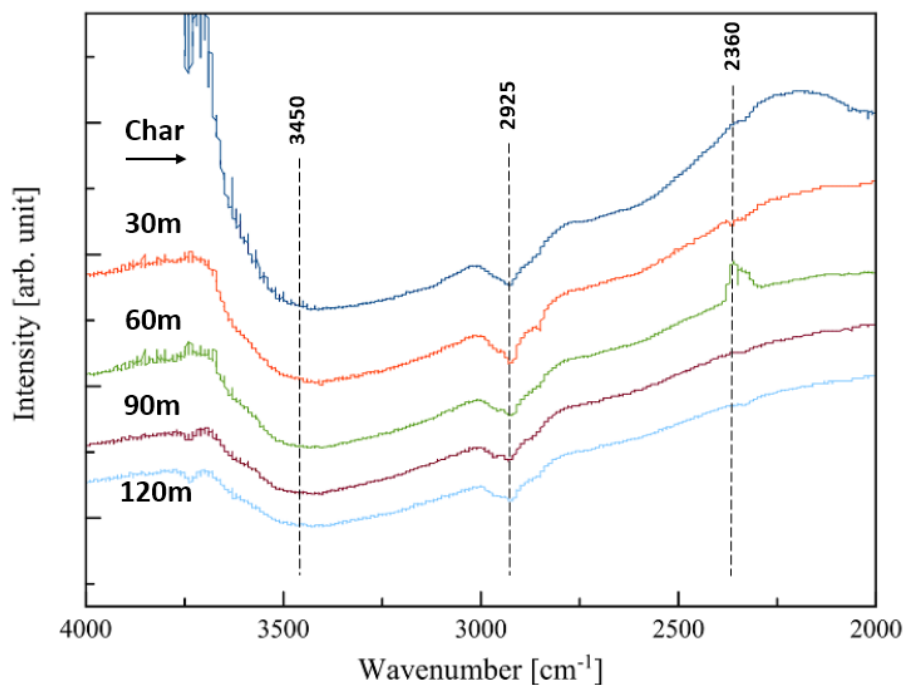
ATR-FTIR spectroscopy, which has better resolution in the fingerprint region (1500-500 cm-1) than DRIFTS is used to analysis. Figure 3 shows the spectra of a different ball milling time series to the DRIFTS one, lacking a 90 minute ball milling. Table # provides the band position and vibrational identity along with the trend in band intensity with ball milling time, while these results are described in depth herein. The sharp band at 1705 cm-1 is the C=O stretching adsorption and represents a variety of C=O containing functional groups, such as carboxylic acid, ester, ketone, or aldehyde groups. This band clearly decreases in intensity with ball milling. At 1609 cm-1 the peak for C=C aromatic ring stretching
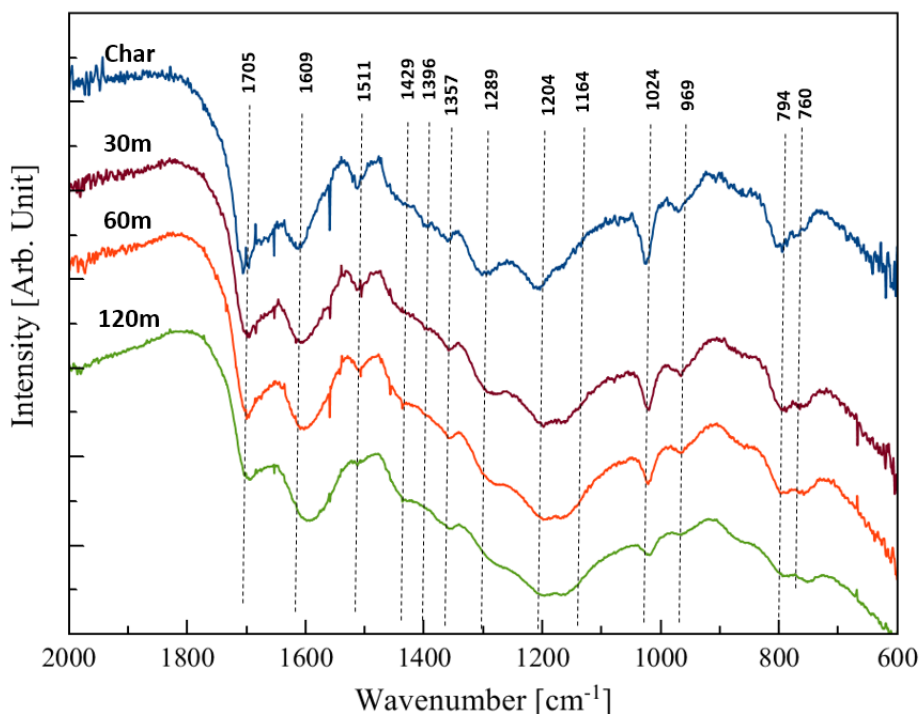
Figure 3: ATR-FTIR of glucose hydrochar ball milling series

increases and shifts downfield. Besides increasing in intensity and shifting, the peak broadens

significantly. The 1600 cm-1 location aligns with adsorptions of carboxylic acid salts and the enol form of

beta-diketones.[Socrates] It is also noteworthy that Zandvoort, in a study of humins, a similar char type

to hydrochar, reported C=C stretching at 1595 cm-1 and attributed this to furan in xylose-derive

humins.[] According to a study by Lund et al, an IR adsorption band at 1500 cm-1 in fructose and glucose

based hydrochars was thought to be HMF (Hydroxymethyl Furfural) within the hydrochar structure.[]

This assumption was made on the basis that the 1505 band was larger for the fructose char than the

glucose char because 5-HMF forms directly from fructose while glucose must isomerize to fructose to

form the compound. Here, the moiety virtually disappears as a result of the 120 minute ball milling,

indicating a shift away from furanic structure. The very small band visible at 1396 cm-1 in the hydrochar

and the 30 minute milling sample represents C-H bending, which went away altogether through the

longer ball millings. The band at 1357 cm-1 indicates aliphatic CH3 deformation and appears to remain

unchanged with ball milling. C-H rocking for olefin carbon is seen at 1289 cm-1 with a clear decrease,

unlike the aliphatic CH3. The sharp, well defined band at 1204 cm-1 represents the C-O bond stretch.

This band does not appear to decrease in intensity with ball milling and broadens with a shift downfield.

The shoulder located at around 1164 cm-1 becomes more absorbing with ball milling and forms into the

bottom of the band at 1204 cm-1 in the 2 hour ball milling. The sharp, strong peak at 1024 cm-1

corresponds to various bond types. It could represent C-O stretching, C-O stretch in a furan ring, or C=C

stretching of an olefin group. The signal strongly decreases with an increasing ball milling time. The peak

at 969 cm-1 shows C-O of ethers and alcohols to decrease significantly with ball milling time. The peaks

at 794 cm-1 and 760 both show decreasing aliphatic and furanic C-H deformations respectively as ball

milling occurs.

The IR analysis hints at decreasing H and O contents or an increasing C content by decreases in C-H and

C-O bonds. This was expected, as reaction conditions heated the vessel and ball milling by its very nature

is a high energy process. When opening the milling vessel after reaction and cooling the vessel there is a

noticeable pressure release, which indicates gas formation. Gas formation was shown in pyrolysis and

related to char formation. [ref] Van Krevelen diagrams for hydrochar formation in Sevilla and Fuertes

indicates the evolution of biomass into hydrochar with reference lines by the reaction of gas formation,

such as demethanation and decarboxylation. [ref] This trend of decreased O and H contents was also

suggested by the decreased water absorbed onto the surface, which was shown by the 3300 cm-1 peak

on the DRIFTS. Less water would attach to the surface because there are fewer oxygen containing

functional groups on the surface for the water to interact with. The structure of hydrochar is shown to

decrease in all structural bonding types except C=C aromatic. This is the only clear cut increase in

structural bond type with ball milling,. The C-O bond shows increase, decrease, no trend, or possibly

decreasing at 4 different C-O peaks. The only increasing trend is based off the shape of a shoulder, but

the trend may be due to a shift down field with the increasing 1024 cm-1 band. C-O bonding is assumed

then to be decreasing. In addition to this C-H rocking for olefin carbon shows this type of bond is present

in the hydrochar with a strong signal and decreases significantly with ball milling. The strength of the

signal suggests that olefin is incorporated into aromatic structures, along with aliphatics.

Table 3: IR band positions and identities for glucose based hydrochar and ball milling products.

Position [cm-1]	Strength	Functional group/Bond Type	Trend
760	m	C-H def. (sub. furans)	None
794	m	C-H def., aliphatic	Decrease
969	w	C-O (ether or alcohols)	Decrease
1024	m	C-O stretch, furan ring or C=C stretching (olefinic groups)	Decrease
1164	sh	C-O (ether or alcohols)	Increase
1204	s	C-O (carboxyl, ester, ether)	None
1289	m	C-H rocking (olefinic)	Decrease
1357	w	CH3 deformation, aliphatic	None
1396	w	C-H bending	Decrease
1511	m	HMF	Decrease
1609	s	C=C aromatic ring stretching	Increase
1705	s	C=O stretching, carbonyl, carboxyl, quinine, ester	Decrease

Raman Analysis

Raman spectra of the D and G peaks region in hydrochar is a source of useful information about the

structure of the carbon material. The Ferrari and Robertson approach, as shown in Figure 4a, poorly fits

the hydrochar with D and G peaks, with the Id/Ig ratio of the intensities of the D and G peaks found to

be 0.58 and increase to .62 with ballmilling, indicating an increase in clustering. These peaks do not

model the hydrochar well, with a significant gap area between the curves and narrowness at the sides.

With ball milling, the D peak shifted up in wavenumber, indicating an increase in olefin chains, either by

length or by amount. The Sadezky fitting shown in Figure 4b shows a significantly improved fitting over

the D/G assumption. The physical meaning behind the disorder peaks is for graphitic species, not chars,

and the actual values for the integrals of the Sadezky peaks are not important on their own but rather

with discussion how these integrals shift with ball milling. These shifts are still unable to be interpreted

as no hydrochar physical equivalents can be explained for the disorder peaks proposed in a graphite
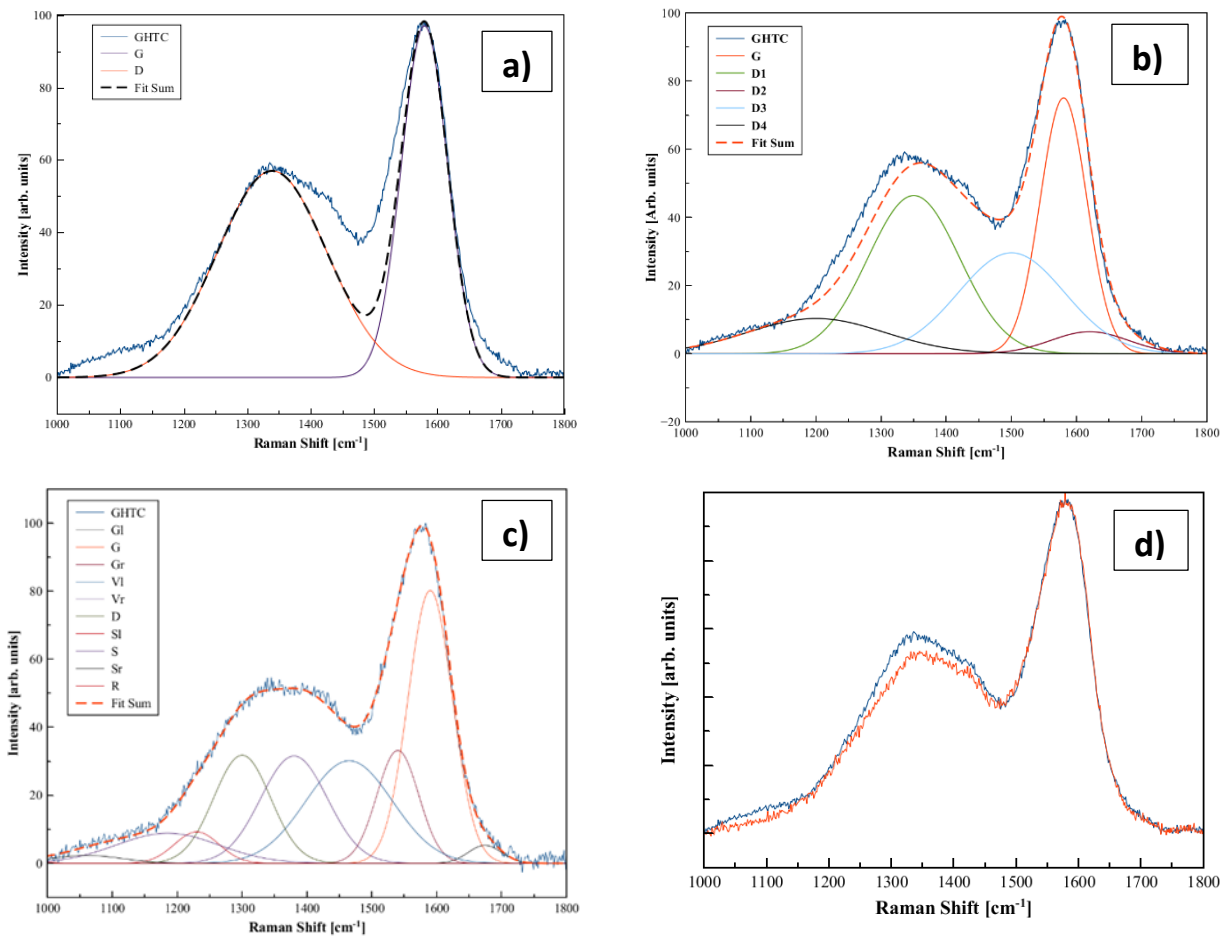
Figure 4. Glucose hydrochar fittings are a) Ferrari and Robertson 2 peak fitting b) Sadezky et. al. 5 peak assignment and c) Li et. al. 10 band assignments. d) is a comparison of glucose hydrochar (blue) and 2 hour ball milled (red).

Table 4: Glucose hydrochar and ball milling Raman peak fitting comparison.

D/G Peak 2-Peak Fitting for Graphite [Ferrari and Robertson]		5-Peak Fitting for soot [Sadezky et al.]		8-Peak Fitting for brown coal [Li et al. 10-PeakFitting]	
GHTC	*GBM (1H)*	*GHTC*	*GBM (1H)*	*GHTC*	*GBM (1H)*
				- (60) R	- (82) R
				322 (51) S_R	207 (52) S_R
		1200 (124) D4	1131 (121) D4	1289 (77) S	1129 (75) S
				661 (38) S_L	944 (29) S_L
1340 (102) D	1357 (115) D	1344 (94) D1	1352 (92) D1	3922 (68) D	3822 (51) D
				2832 (60) V_L	3995 (69) V_L
				5700 (60) V_R	5200 (66) V_R
		1507 (77) D3	1505 (62) D3	228 (60) G_L	187 (55) G_L
1580 (43) G	1589 (43) G	1581 (51) G	1590 (45) G	6790 (47) G	7205 (50) G
		1670 (58) D2	1699 (114) D2	3184 (60) G_R	2340 (116) G_R

Raman Analysis Continued

species. The lack of applicability of Sadezki et al model to ball milling of hydrochar is the small shifts seen in Figure 4d at 1100 and 1350. The small shifts correspond to the D1 and D4 peaks respectively. The D1 peak represents graphite edges, which could be also be considered as small aromatic clusters as both exhibit the A1g breathing mode. This shows an increase with ball milling which is expected. In addition the D4 peak increased, which could be interpreted (according to Sadezki) as an increase in polyenes. This is unexpected and could be due to intermolecular dehydration reactions. [sevilla] The Li fitting integral values are listed in Table 4, with the HWHM shown in parentheses. The R band was not assigned. The biggest changes are decreases to Gr, Sr, and Vr, and increases to Vl, Sl, and G. Gr, Sr and Vr are amorphous aromatics, methyl groups, and aromatic rings. Since Vl increased and Vr decreased and they represented the same thing except for the methylene, this was the factor that caused the increase. The Gr decrease is for aromatics with 3-5 rings or amorphous while G is alkene C=C. This suggests that aromatic rings are either falsely represented in Raman spectroscopy or ball milling, a high energy process, is not actually making the carbon aromatic as previously thought. This may be that the formation of aromatic with ball milling is simply such a small part of the process, and perhaps a lot of the chemistry takes place because of the temperature and instability of the material. Ball milling can break C-C bonds but perhaps the prevalence of weaker bonds such as ether linkages are driving the formation of olefin groups. The aromatics with 3-5 rings could refer to furan rings that are close and haven't broken. This is supported by bond breaking attributed to furan rings in the IR.

Xylose Hydrochar Ball Milling Study

Figure 4: ATR-FTIR of Xylose Char and 60 m ball milled xylose char
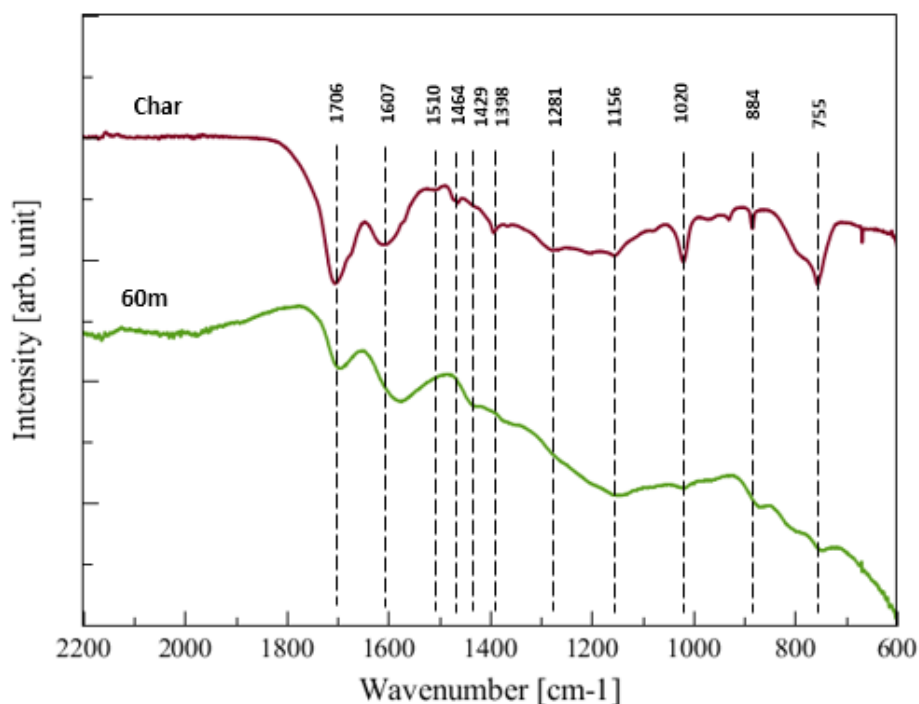
Xylose samples, when subjected to a 1 hour ball milling, showed significantly lower IR activity at most band sites, which was noticeable in the glucose chars but not to the same degree. The IR absorption increases as the wavenumber decreases for the ball milled sample. The xylose char shows excellent IR absorption in terms of easy to determine whether bands exist at a given location. These trends may be accurate due to the difficult of scaling the two spectra such that the band absoprtion intensities can be simply compared. Band assignments used van Zandvoort et al, Sevilla et al, Fuertes et al, and Socrates. []

With ball milling, xylose hydrochar, oxygen containing functional groups decrease sharply at 1705 and 1020 cm-1, corresponding to C=O stretching and C-O stretching or furan ring or olefinic C=C stretching. The absorption at 1020 cm-1 is hardly noticeable as a result of the ball milling. Band increases were seen for 1607, 1156, and maybe 884 cm-1, corresponding to C=C aromatic ring stretching, C=C ring stretching, C-O corresponding to ether or alcohols, and C-H deformation for CH2. Substituted furan decreases were seen with the disappearence of the peak at 1020 cm-1 and the decrease in the peak at 1510 cm-1 for aromatic ring stretching on substituted furans. C-H functionalities at 1464, 1398, 1281, and 755 cm-1 all

decrease through the ball milling. The disappearance of furan is further solidified by the sharp decrease in the band at 755 cm-1 which corresponds to C-H deformation in substituted furans.

Table 5: IR band positions and Functional Assignment for xylose based hydrochar and milling products

Position [cm-1]	Strength	Functional group/Bond Type	Trend
755	s	C-H def. (sub. furans)	None
884	w	C-H def., aliphatic	Decrease
1020	m	C-O stretch, furan ring or C=C stretching (olefinic groups)	Decrease
1156	m	C-O (ether or alcohols)	Increase
1281	m	C-O (carboxyl, ester, ether)	None
1398	w	C-H rocking (olefinic)	Decrease
1429	w	CH3 deformation, aliphatic	Increase
1464	w	C-H bending	Decrease
1510	vw	HMF	Decrease
1607	s	C=C aromatic ring stretching	Increase
1706	s	C=O stretching, carbonyl, carboxyl, quinine, ester	Decrease

Figure 5: DRIFTS Comparison of Xylose Hydrochar (orange) and 1 hour ball milled xylose char (green)
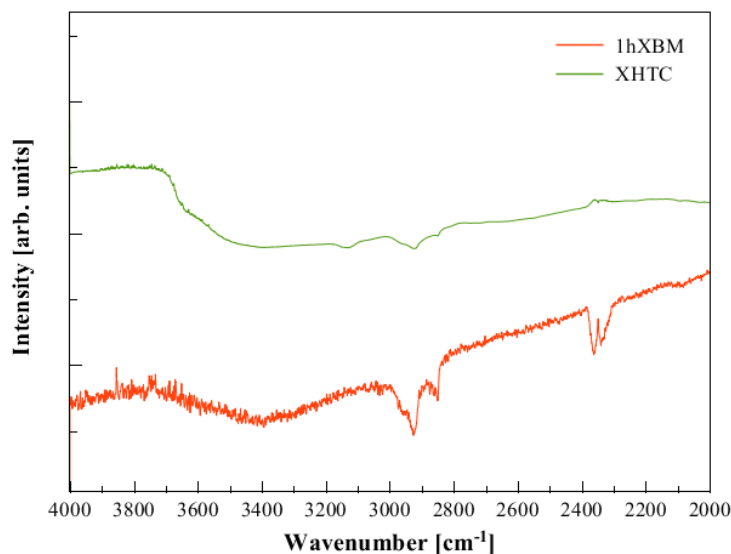
Conclusion

IR spectroscopy was successful in the ability to track changes in hydrothermal carbon as the material was ball milled and showed changes between hydrochar with an alternate structure. The experiments showed deoxygenation of the hydrochar, a decrease in alkyl groups, and an increase in olefin structures. The drop in aromaticity with ball milling was proposed to be a result of furan ring degredation. Differences in sugar types were indicated with a higher olefin content in hydrochar as well as an increased presence of C-O bonds. Ball milling processes vary significantly between xylose and glucose hydrochars, with xylose displaying a greater degree of aromaticity in the ball milling products than glucose. Future work will seek to explain these changes through atomic mass spectroscopy and how hydrochars and ball milling products behave as a result of functionalization.

Acknowledgements

Sources

1) Canadell, J. G., C. Le Quéré, M. R. Raupach, C. B. Field, E. T. Buitenhuis, P. Ciais, T. J. Conway, N. P. Gillett, R. A. Houghton, and G. Marland. "From the Cover: Contributions to Accelerating Atmospheric CO2 Growth from Economic Activity, Carbon Intensity, and Efficiency of Natural Sinks." *Proceedings of the National Academy of Sciences* 104.47 (2007): 18866-8870.

2) Hoffert, Martin I., Ken Caldeira, Atul K. Jain, Erik F. Haites, LD Danny Harvey, Seth D. Potter, Michael E. Schlesinger et al. "Energy implications of future stabilization of atmospheric CO2 content." *Nature* 395, no. 6705 (1998): 881-884.

3) Houghton, John T., L. G. Meira Filho, B. A. Callander, N. Harris, and A. Kattenberg. "Climate change 1995: the science of climate change." (1996).

4) Karl, Thomas R., and Kevin E. Trenberth. "Modern global climate change." *science* 302, no. 5651 (2003): 1719-1723.

5) Solomon, Susan, Gian-Kasper Plattner, Reto Knutti, and Pierre Friedlingstein. "Irreversible climate change due to carbon dioxide emissions." *Proceedings of the national academy of sciences* 106, no. 6 (2009): 1704-1709.

6) Schmalensee, Richard, Thomas M. Stoker, and Ruth A. Judson. "World carbon dioxide emissions: 1950–2050." *Review of Economics and Statistics* 80, no. 1 (1998): 15-27.

7) Cohen, Joel E. "Human population: the next half century." *science* 302, no. 5648 (2003): 1172-1175.

8) Balat, Mustafa, and Havva Balat. "Recent trends in global production and utilization of bio-ethanol fuel." *Applied Energy* 86, no. 11 (2009): 2273-2282.

9) Brennan, Liam, and Philip Owende. "Biofuels from microalgae—a review of technologies for production, processing, and extractions of biofuels and co-products." *Renewable and sustainable energy reviews* 14, no. 2 (2010): 557-577.

10) Le Quéré, Corinne, Michael R. Raupach, Josep G. Canadell, Gregg Marland, Laurent Bopp, Philippe Ciais, Thomas J. Conway et al. "Trends in the sources and sinks of carbon dioxide." *Nature Geoscience* 2, no. 12 (2009): 831-836.

11) Stöcker, Michael. "Biofuels and biomass-to-liquid fuels in the biorefinery: Catalytic conversion of lignocellulosic biomass using porous materials." *Angewandte Chemie International Edition* 47, no. 48 (2008): 9200-9211.

12) Mohan, Dinesh, Charles U. Pittman, and Philip H. Steele. "Pyrolysis of wood/biomass for bio-oil: a critical review." *Energy & Fuels* 20, no. 3 (2006): 848-889.

13) Naik, S. N., Vaibhav V. Goud, Prasant K. Rout, and Ajay K. Dalai. "Production of first and second generation biofuels: a comprehensive review." *Renewable and Sustainable Energy Reviews* 14, no. 2 (2010): 578-597.

14) Kamm, Birgit, Patrick R. Gruber, and Michael Kamm. "Biorefineries–industrial processes and products." *Ullmann's Encyclopedia of Industrial Chemistry* (2007).

15) Gomez, Leonardo D., Clare G. Steele-King, and Simon J. McQueen-Mason. "Sustainable liquid biofuels from biomass: the writing's on the walls." *New Phytologist* 178, no. 3 (2008): 473-485.

16) Bahng, Mi-Kyung, Calvin Mukarakate, David J. Robichaud, and Mark R. Nimlos. "Current technologies for analysis of biomass thermochemical processing: a review." *Analytica Chimica Acta* 651, no. 2 (2009): 117-138.

17) Onda, Ayumu, Takafumi Ochi, and Kazumichi Yanagisawa. "Selective hydrolysis of cellulose into glucose over solid acid catalysts." *Green Chemistry* 10, no. 10 (2008): 1033-1037.

18) Hara, Michikazu, Takemi Yoshida, Atsushi Takagaki, Tsuyoshi Takata, Junko N. Kondo, Shigenobu Hayashi, and Kazunari Domen. "A carbon material as a strong protonic acid." *Angewandte Chemie International Edition* 43, no. 22 (2004): 2955-2958.

19) Sevilla, Marta, and Antonio B. Fuertes. "Chemical and structural properties of carbonaceous products obtained by hydrothermal carbonization of saccharides." *Chemistry-A European Journal* 15, no. 16 (2009): 4195-4203.

20) Heckley, Erin, Toto, Josh, and Venegas, Juan. "The Structural Changes of Hydrothermally Treated Biochar Caused By Ball-Milling." MQP report., Worcester Polytechnic Institute, 2014.

21) Brown, Robert C. 2011. "Introduction to Thermochemical Processing of Biomass into Fuels, Chemicals, and Power." In *Thermochemical Processing of Biomass Conversion into Fuels, Chemicals and Power*, edited by Robert C. Brown, 1-12. Chichester, West Sussex, United Kingdom: Wiley.

22) Socrates, George. *Infrared and Raman characteristic group frequencies: tables and charts*. John Wiley & Sons, 2004.

23) Guo, Haixin, Xinhua Qi, Luyang Li, and Richard L. Smith. "Hydrolysis of cellulose over functionalized glucose-derived carbon catalyst in ionic liquid." *Bioresource technology* 116 (2012): 355-359.

24) van Zandvoort, Ilona, Yuehu Wang, Carolus B. Rasrendra, Ernst RH van Eck, Pieter CA Bruijnincx, Hero J. Heeres, and Bert M. Weckhuysen. "Formation, molecular structure, and morphology of humins in biomass conversion: influence of feedstock and processing conditions." *ChemSusChem* 6, no. 9 (2013): 1745-1758.

25) Wang, Meijun, Daniel G. Roberts, Mark A. Kochanek, David J. Harris, Liping Chang, and Chun-Zhu Li. "Raman spectroscopic investigations into links between intrinsic reactivity and char chemical structure." *Energy & Fuels* 28, no. 1 (2013): 285-290.

26) Sadezky, Alexa, Harald Muckenhuber, Hinrich Grothe, R. Niessner, and Ulrich Pöschl. "Raman microspectroscopy of soot and related carbonaceous materials: spectral analysis and structural information." *Carbon* 43, no. 8 (2005): 1731-1742.

27) Ferrari, A. C., and J. Robertson. "Interpretation of Raman spectra of disordered and amorphous carbon." *Physical review B* 61, no. 20 (2000): 14095.

28) Cuesta, A., P. Dhamelincourt, J. Laureyns, A. Martinez-Alonso, and JM Diaz Tascón. "Raman microprobe studies on carbon materials." *Carbon* 32, no. 8 (1994): 1523-1532.

Appendix

Reproducibility of Hydrochars

As mentioned in the results section, hydrochar reproducibility was difficult to attain. This uncertainty is not well illustrated through the portrayal of singular data sets. The variability of chars produced under assumedly identical condition manifests with different changes on different instruments. These changes are highlighted for the different materials (glucose char, glucose char ball milled, xylose char, glucose char ball milled) and the instruments used (ATR-FTIR, DRIFTS, and Raman).

Glucose

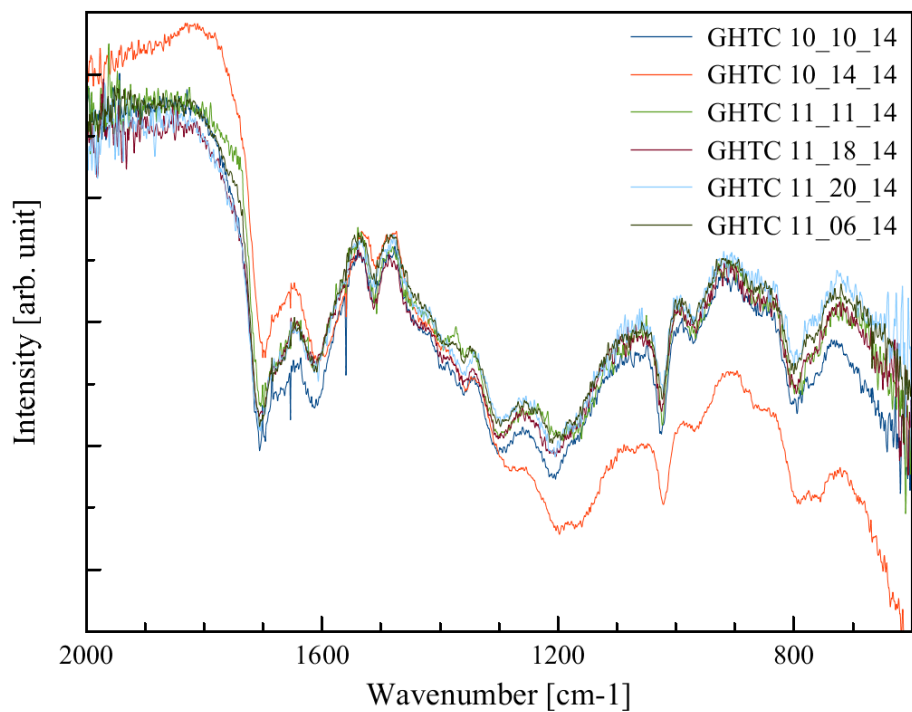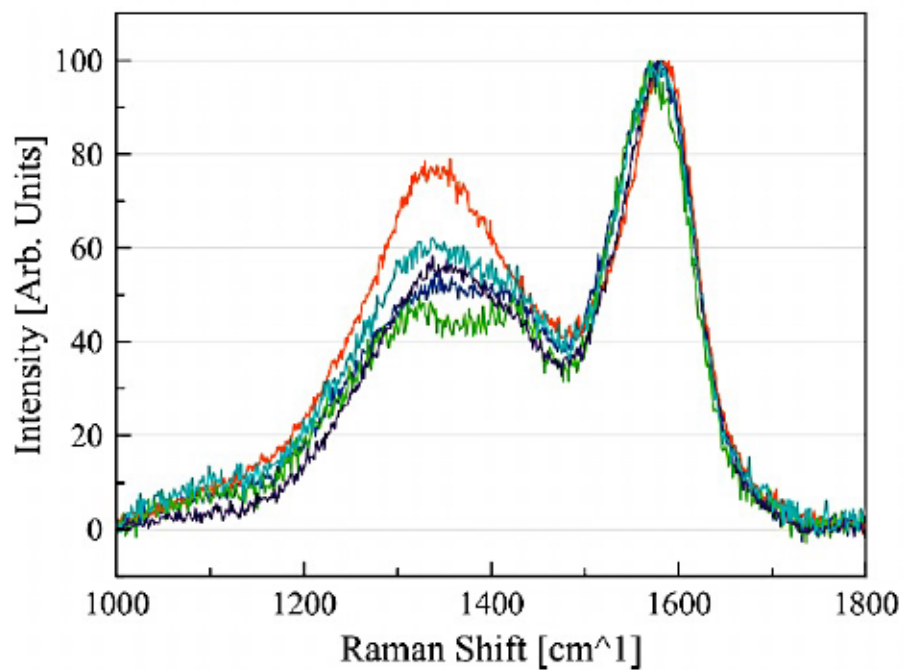*Figure 6: Glucose Hydrochar Reproducibility Plot for ATR-FTIR*

Figure 7: Hydrochar Reproducibility Plot for Raman Spectroscopy.
Adapted from Heckley et. al.

Xylose

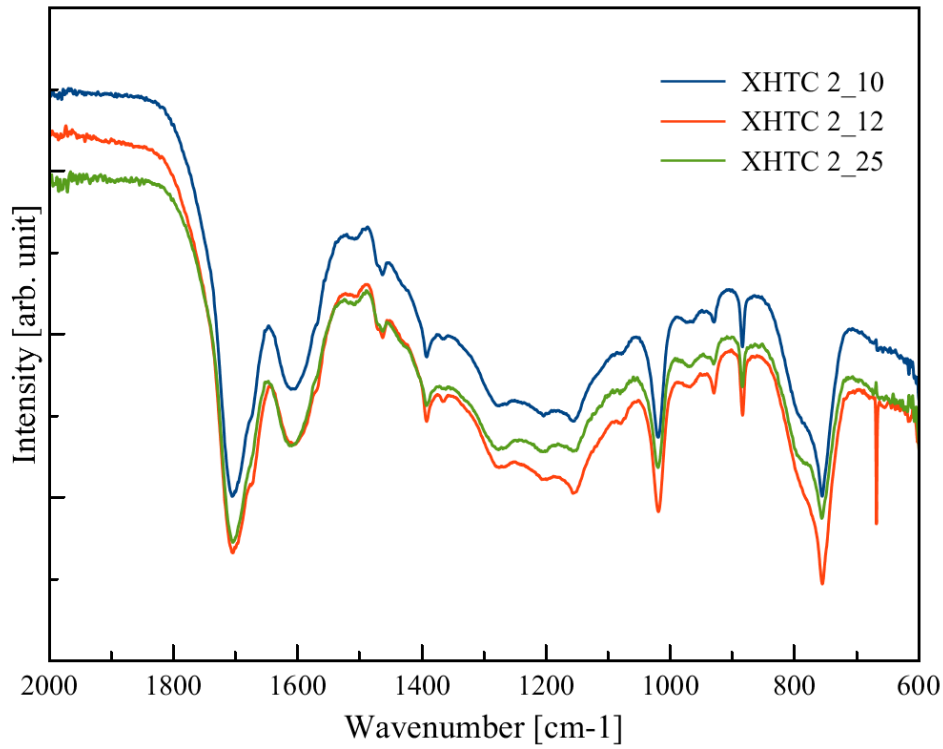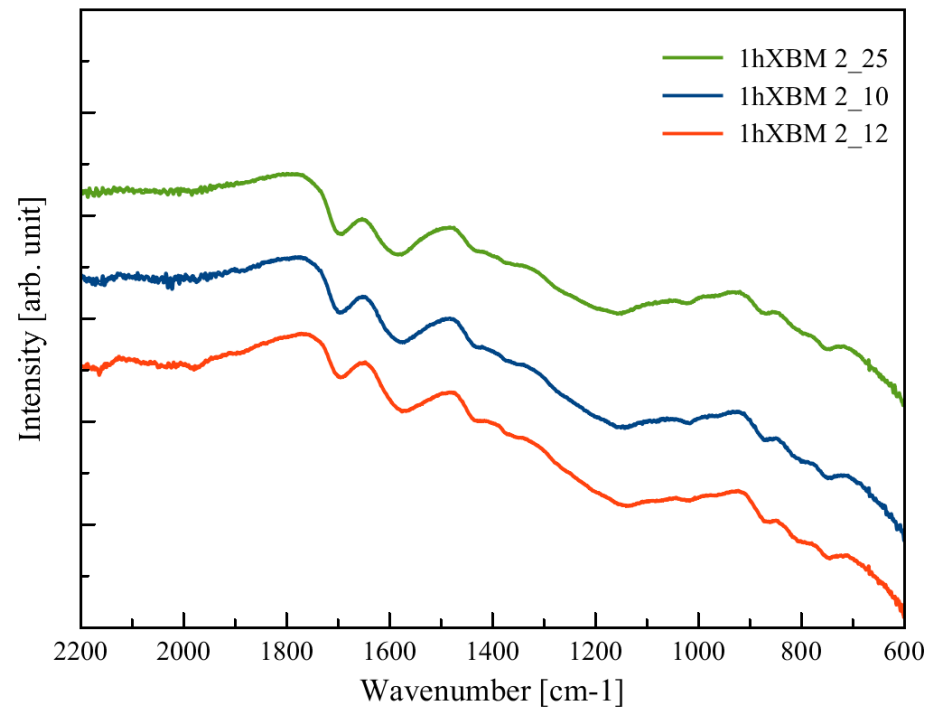*Figure 8:Reproducibility of Xylose HTC- analyzed with ATR-FTIR*

Figure 9::Reproducibility of Ball Milled Xylose HTC- analyzed with ATR-FTIR

Xylose Chars

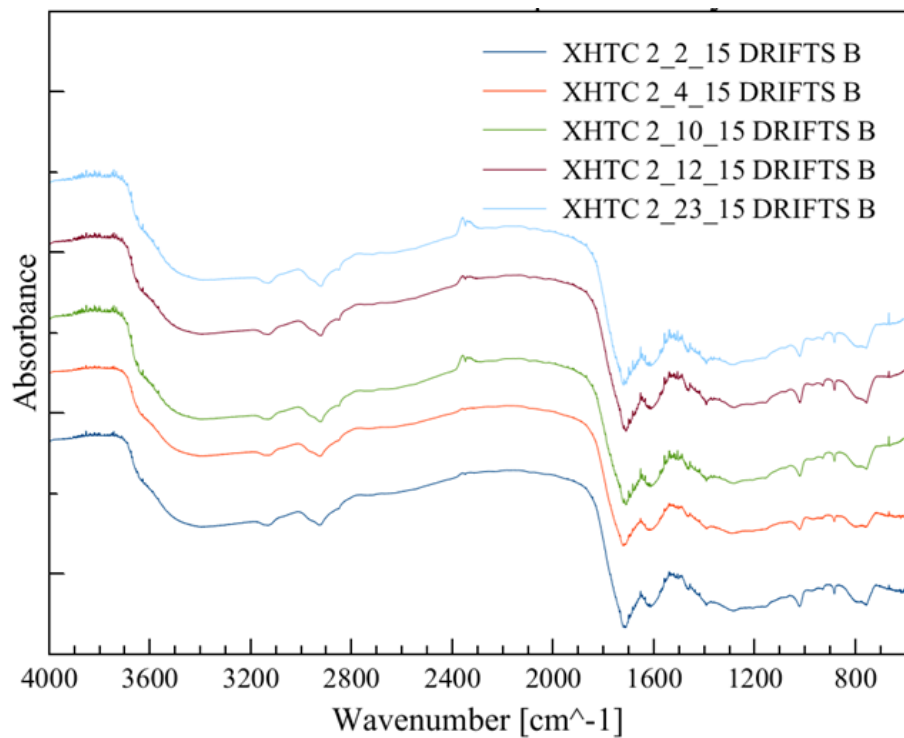*Figure 10: Reproducibility of Xylose HTC- analyzed with DRIFTS*

Figure 11: Reproducibility of ball milled Xylose HTC- analyzed with DRIFTS
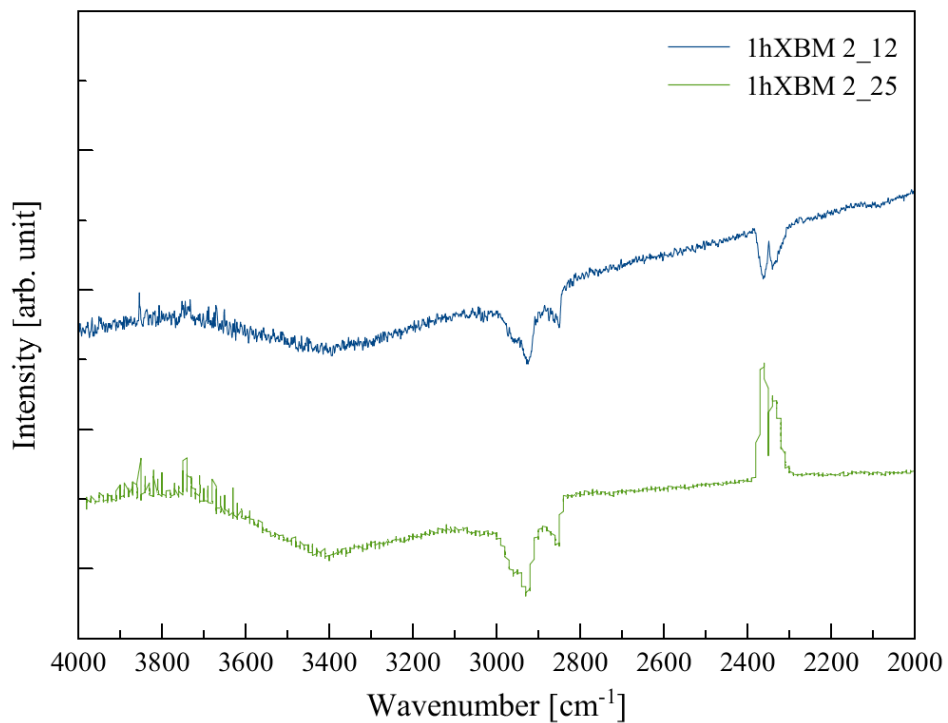
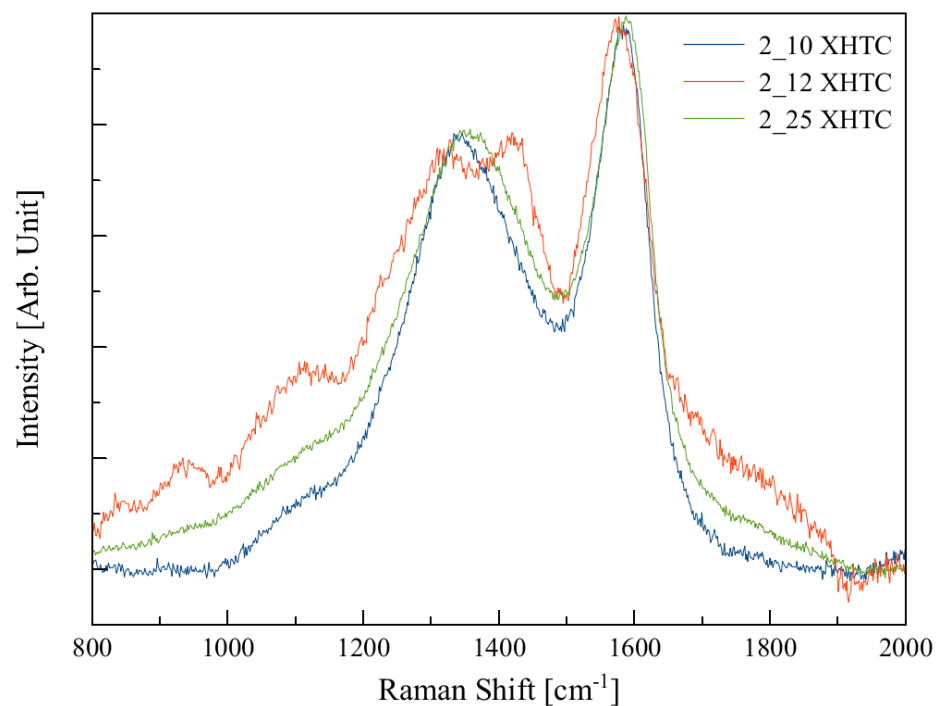*Figure 12: Reproducibility of Xylose HTC- analyzed with Raman Spectroscopy*

Figure 13:Reproducibility of ball milled Xylose HTC- analyzed with Raman Spectroscopy